PAPER

A high-performance *n*-butanol gas sensor based on ZnO nanoparticles synthesized by a low-temperature solvothermal route†

Xu Liu,[a] Nan Chen,[a] Xinxin Xing,[a] Yuxiu Li,[a] Xuechun Xiao,[ab] Yude Wang*[ab] and Igor Djerdj*[c]

ZnO nanoparticles with high crystallinity and several nanometers in size were synthesized by a low-temperature solvothermal route from zinc acetate dihydrate ($Zn(CH_3COO)_2 \cdot 2H_2O$), potassium hydroxide (KOH) and methanol (CH_3OH). The structural and the morphological characterizations of the ZnO nanoparticles were performed by X-ray powder diffraction (XRD), transmission electron microscopy (TEM), X-ray photoelectron spectroscopy (XPS) and N_2-sorption isotherms. The obtained nanoparticles are highly crystalline wurtzite-type ZnO with a uniform near-spherical shape and an average particle size estimated to be 8.4 ± 1.3 nm. Such a small particle size and slight agglomeration are attributed to the use of methanol, which acts as both a solvent and an inhibitor of growth and agglomeration. The as-synthesized ZnO nanoparticles were directly used as a gas sensing material toward *n*-butanol gas. Such a designed sensor device exhibits several advantages such as a high and fast response, short recovery time, and good stability toward *n*-butanol gas. At the optimal operating temperature (320 °C), its gas response toward 500 ppm *n*-butanol is 805 and the response and recovery times are 22 and 6 seconds, respectively.

1. Introduction

Volatile organic compounds (VOCs) are a group of chemical compounds that easily evaporate at room temperature.[1] They are not only harmful for the environment but also considered to seriously affect human health and security.[2] For instance, *n*-butanol, an important solvent, organic synthesis raw material and extracting agent, is widely used in laboratories and factories. Such an agent is a stimulating and narcotic liquid. Exposure to *n*-butanol vapour could cause several symptoms such as

headache, dizzy, drowsiness, dermatitis and discomfort of the eyes, nose, as well as the throat.[3] Many countries' specified threshold limit value of *n*-butanol in the work place is only 152–304 mg m^{-3}, such as 200 mg m^{-3} for China, 304 mg m^{-3} for the Occupational Safety and Health Administration (OSHA), 152 mg m^{-3} for the American Conference of Governmental Industrial Hygienists (ACGIH), and so on. Moreover, *n*-butanol is also inflammable. An air mixture which contains 1.45–11.25% *n*-butanol by volume may cause an explosion or flash fire at a temperature higher than its flash point (35 °C). Its product of combustion contains CO and CO_2 which are suffocating gases. Thus, high performance sensors to monitor *n*-butanol for laboratories and factories are needed. Compared with traditional methods such as chromatography,[3] semiconductor metal oxide-based gas sensors are thought to be the most promising miniaturized gas-sensing devices owning to their high sensitivity, fast response, low cost and small size.

As one of the most versatile semiconductor materials, the wurtzite-type ZnO, with a wide band gap energy (3.37 eV) and very large excitation binding energy (60 meV) at room temperature,[4] plays an important role in various technological domains such as solar cells,[5] spintronic devices,[6] photodetectors,[7] light emitting diodes,[8] and nanolasers,[9] owing to the combination of optical and electrical properties. ZnO is also an excellent substance used for the detection of VOCs due to its low cost, high sensitivity and quick gas recovery.[10,11] It is known that the morphology has a great influence on the gas sensing

[a]*School of Physics Science and Technology, Yunnan University, 650091 Kunming, People's Republic of China*

[b]*Yunnan Province Key Lab of Micro-Nano Materials and Technology, Yunnan University, 650091 Kunming, People's Republic of China. E-mail: ydwang@ynu.edu.cn; Fax: +8687165153832; Tel: +8687165031124*

[c]*Ruđer Bošković Institute, Bijenička 54, 10000 Zagreb, Croatia. E-mail: igor.djerdj@irb.hr; Fax: +38514680114; Tel: +38514680113*

† Electronic supplementary information (ESI) available: Table S1 structural and microstructural parameters extracted from the Rietveld refinement of powder XRD pattern; Fig. S1 cross section and surface SEM images of the sensors; Fig. S2 (a) a photograph of the WS-30 A testing system, (b) the basic testing principle, (c) the schematic structure of the gas sensor, and (d) the picture of a completed gas sensor; Fig. S3 variation of resistance with temperature; Fig. S4 gas response of the as-fabricated gas sensor toward 500 ppm *n*-butanol gas tested at different temperatures; Fig. S5 dynamic response curves of the as-fabricated sensor toward ethanol, acetone and isopropanol at 320 °C; Fig. S6 the high-resolution XPS spectra of (a) Zn2p and (b) O1s of ZnO nanoparticles. See DOI: 10.1039/c5ra05148g

properties of materials,[12] and a composite of a noble metal[13] or other metal oxide[11] can significantly increase their gas sensing properties. Up to now, a lot of different morphological ZnO and ZnO-based composites have been prepared and used for detecting *n*-butanol such as ZnO nanoflakes,[14] ZnO nanowires,[15] ZnO microflowers,[16] Au-functionalized porous ZnO microsheets,[17] ZnO-decorated α-Fe$_2$O$_3$,[18] and so on. Though they have a better gas response toward *n*-butanol than other metal oxide semiconductors (*e.g.*, SnO$_2$ nanospheres,[19] α-Fe$_2$O$_3$ hollow spindles,[20] ZnSnO$_3$ nanocubes,[21] WO$_3$ nanoflowers,[22] NiO hollow spheres,[23] and so on), the performances including sensitivity, selectivity, response and recovery times for *n*-butanol detection are still not ideal. A high sensing material for the detection of *n*-butanol gas is still to be developed. Recent contributions have shown that these performance indexes could be improved by a smaller grain size, which will result in a higher specific surface area.[16,24] Therefore, well crystallized ZnO nanoparticles with a small grain size ought to have good gas sensing properties.

This paper describes a simple low-temperature solvothermal route to ZnO nanoparticles with high crystallinity for gas sensing purposes. The obtained ZnO nanoparticles were used to fabricate a gas sensor which shows high sensitivity, good selectivity, a fast response and recovery, and good repeatability and stability toward *n*-butanol gas. The structure, morphology, chemical state, and specific surface area were also investigated to give a further understanding of related nanocrystal formation and gas sensing mechanisms.

2.   Experimental

2.1.   Preparation of ZnO nanoparticles

All the chemical reagents used in the experiments were obtained from commercial sources as guaranteed-grade reagents and used without further purification.

ZnO nanoparticles were prepared by a simple low-temperature solvothermal method. In a typical synthetic experiment, 0.5817 g of Zn(CH$_3$COO)$_2$·2H$_2$O and 0.2700 g of KOH were dissolved into 25 mL and 15 mL methanol respectively, to get transparent solutions. Later, the solution of potassium hydroxide was poured into zinc acetate solution to form a white suspension. The pH of the suspension was measured to be 8. After magnetically stirring for 20 min, 33 mL of the mixture was transferred into a Teflon-lined stainless steel autoclave with a capacity of 55 mL and reacted under solvothermal conditions at 100 °C for 4 h. The autoclave was cooled down to room temperature in a standard atmosphere. The resulting product was centrifuged, and the white precipitate was thoroughly washed with ethanol and dried at 60 °C overnight. The reaction yield was estimated to be 81.3%.

2.2.   Characterization

X-Ray diffraction (XRD, Rigaku D/MAX-3B powder diffractometer) with a copper target and K$_\alpha$ radiation ($\lambda = 1.54056$ Å) was used for the phase identification, where the diffracted X-ray intensities were recorded as a function of 2θ. The sample was

scanned from 10° to 90° (2θ) in steps of 0.01°. The transmission electron micrographs were obtained with a Zeiss EM 912 Ω instrument at an acceleration voltage of 120 kV, while high-resolution transmission electron microscopy (HRTEM) characterization was done using a Philips CM200-FEG microscope (200 kV, $C_s = 1.35$ mm). The samples for TEM were prepared by dispersing the final dry powders in ethanol; this dispersion was then dropped on carbon–copper grids. The nitrogen adsorption isotherm was measured at 77.3 K with a Micromeritics ASAP 2010 automated sorption analyzer. Prior to the measurement, the sample was degassed at 300 °C for 3 h under a vacuum. X-ray photoelectron spectroscopy (XPS) was carried out at room temperature in an ESCALAB 250 system. During XPS analysis, an Al Kα X-ray beam was adopted as the excitation source and the vacuum pressure of the instrument chamber was 1×10^{-7} Pa, as read on the panel. The measured spectra were decomposed into Gaussian components by a least-square fitting method. Bonding energy was calibrated with reference to the C1s peak (285.0 eV).

2.3.   Fabrication and measurement of the gas sensor

The test gas sensor system was fabricated according to the literature.[25] At the very beginning, the as-synthesized products were mixed with deionized water to form a paste. Afterwards, the paste was coated by a paint pen onto the outside surface of an alumina tube (4 mm in length, 1.2 mm in external diameter, and 0.8 mm in internal diameter) with a pair of Au electrodes at each end connected by platinum wires. The thickness of the gas sensing materials was about 54 μm to uniformly cover all of the Au electrodes to guarantee good contact (Fig. S1†). Next, the sensors were calcined in air at 400 °C for 2 h and then a Ni–Cr heating wire was inserted in the tube to control the operating temperature *via* a heating voltage (V_h), as shown in Fig. S2.† In order to improve the stability and repeatability, the fabricated sensors were aged at 320 °C for 48 h in air. Finally, the sensors were well connected to a bakelite base through platinum wires to perform electrical measurements using a WS-30A system (Weisheng Instruments Co. Zhengzhou, China, as shown in Fig. S2†). During the testing process, the desired amounts of the target substance were injected into the chamber by a micro-syringe after the resistances of all the sensors were stable. The analyte solution was evaporated by a quick evaporator and mixed with air immediately by two installed fans in the chamber (18 L in volume). The gas response β was defined as the ratio of the electrical resistance in air (R_0) to that in gas (R_g). In addition, the response time was defined as the time required for the gas response to reach 90% of the final equilibrium value after a test gas was injected, and the recovery time was the time needed for gas response to decrease by 90% after the gas sensor was exposed in air again.

3.   Results and discussion

The structural and microstructural features of the as-prepared ZnO nanoparticles were analyzed by the X-ray diffraction (XRD). The initial assignment was further confirmed by the

refinement of the diffraction pattern with the Rietveld method. The experimental pattern, together with the calculated pattern obtained from the Rietveld refinement and difference profile thereof are shown in Fig. 1. The difference curve between the calculated and experimental XRD patterns indicates an excellent agreement. The present diffraction peaks in the powder pattern illustrate high crystallinity of the products of a wurtzite-type ZnO structure (ICDD PDF no. 80-0074), space group $P6_3mc$ (186). No diffraction peaks belonging to any other compound were found, demonstrating the high purity of the obtained product. Due to the broadening of the diffraction peaks, the overlapping of neighboring peaks can be observed, such as the overlapping of (200), (112) and (201). The volume-weighted average crystallite size calculated from the Rietveld profile refinement is 6.9 nm. The other structural parameters obtained from the Rietveld profile refinement such as unit cell parameters, fractional atomic coordinates, and microstrain are listed in Table S1.†

The morphology and the size distribution of the as prepared powder were further examined with transmission electron microscopy (TEM), as shown in Fig. 2. From Fig. 2(a), one can observe that the particles with small agglomerates have a rather uniform near-sphere shape as well as size. The clear lattice fringes displayed in Fig. 2(b) demonstrate the high crystallinity and random orientation of the ZnO nanoparticles. A high-resolution TEM image of an isolated ZnO nanocrystal is also shown in Fig. 2(c). The interplanar spacing is estimated to be 0.282 nm, which corresponds to the (100) lattice plane of ZnO, and the size of such a well-defined particle can be easily measured to be 8.7 nm. Furthermore, the size distribution curve of the nanoparticles was obtained by measuring several hundred nanocrystals from the HRTEM images and is shown in Fig. 2(d). The statistic result, 8.4 ± 1.3 nm, has a good agreement with the result of the XRD. Both of them demonstrate that

the as-synthesized ZnO nanoparticles do have a small grain size and the specific surface area estimated from the BET method is 81.0 m^2 g^{-1}.

In general, ZnO is very easy to crystallize even in pretty facile situations. For instance, 90 °C and 1.5 h are enough to obtain micron-sized ZnO crystals from the mixed aqueous solution of $Zn(NO_3)_2$ and hexamethylenetetramine.[26,27] Moreover, high agglomerations are always observed in nanocrystals owing to the high surface energy, which is the nature of nanomaterials.[28] When the particle size is smaller, more serious agglomerations occur. However, the ZnO nanoparticles prepared under solvothermal conditions at 100 °C for 4 h in this work, not only have a small grain size but also have slight agglomerations. These are attributed to the use of methanol, which acts as both a solvent and a crystal growth inhibitor, instead of water and other alcohols. The formation process of the slight-agglomeration nanoscaled ZnO nanocrystalline particles is schematically illustrated in Fig. 3. At the beginning, zinc acetate and potassium hydroxide ionize Zn^{2+} and OH^- in the corresponding solution. Once the solution of potassium hydroxide is added to zinc acetate solution, the ionized Zn^{2+} and OH^- will react to form $Zn(OH)_2$. The formation of ZnO crystal nuclei from the formed $Zn(OH)_2$ is a complicated process, but it mainly relies on the dehydration of hydroxyl belonging to $Zn(OH)_2$.[29,30] At the surface of the ZnO crystal nuclei, the bonding hydroxide ions form hydrogen bonds with methanol, and the methyl which shows positive electricity points to the solvent. Such a positively charged surface will repel the other equally positively charged nuclei. And the methyl is stable with $Zn(OH)_2$, which
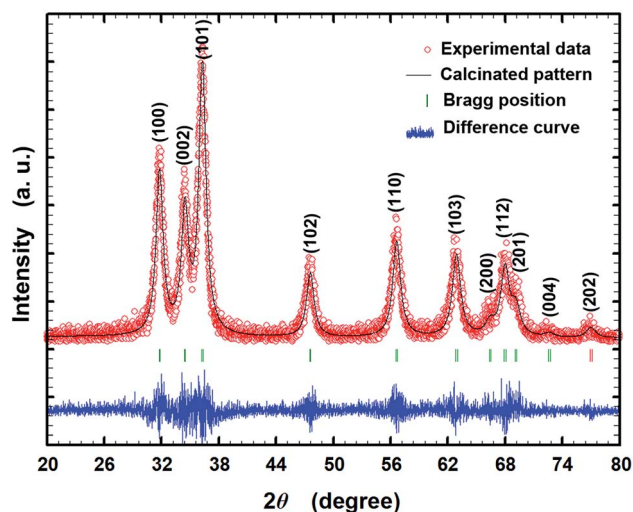

Fig. 1 Typical Rietveld output plot of the as-prepared ZnO nano-particles. The experimental data is shown in red, the calculated pattern in black, and the difference curve in blue. The short vertical bars in green represent the positions of the Bragg reflections.
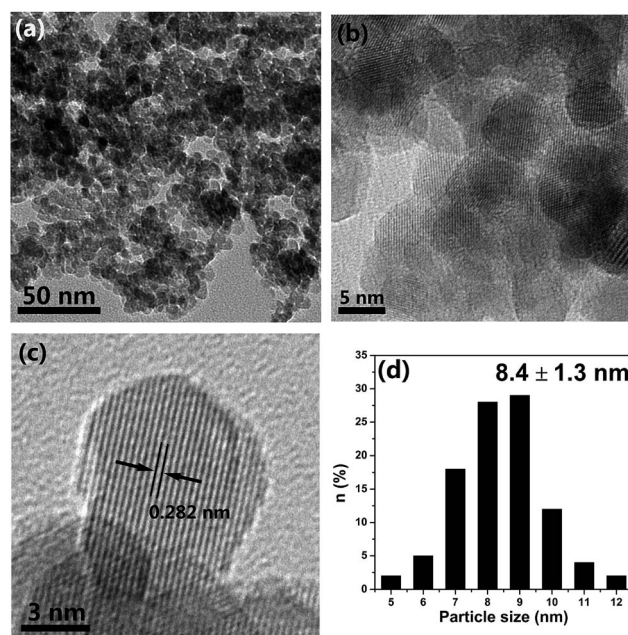

Fig. 2 TEM image (a), HRTEM image (b) of the ZnO nanoparticles, HRTEM image of an isolated ZnO nanoparticle (c), and the size distribution of the ZnO nanoparticles obtained by measuring the size of more than one hundred ZnO nanoparticles from the HRTEM images (d).

acts as an inhibitor to limit the growth of the ZnO nuclei. This mean that methanol, used as a solvent in this work, also acts as an inhibitor to limit the growth and agglomeration of ZnO, and further leads to the slight-agglomeration of nanoscaled ZnO. Generally, water and some other longer carbon link alcohols are used as solvents for ZnO preparation. Owing to a similar structure, all of them can form hydrogen bonds with the capped ZnO nuclei, but the tiny differences in structure between them and methanol make water and other long C link alcohols less suitable in inhibiting the growth and agglomeration of ZnO particles. Water molecules have a stronger hydrogen bond with the hydroxyl bonding to the surface of ZnO nuclei than methanol, but H_2O easily ionizes to a hydroxyl and proton. The ionization of H_2O will cause the opposite charge of the nuclei and proton transfer between the ZnO nuclei. As for other longer C link alcohols, the longer C link weakens the hydrogen bond, which results in a weaker inhibition. This makes methanol the most suitable agent to synthesize ZnO nanoparticles with slight agglomerations. We recently reported that the size of ZnO quantum dots can be tuned by different alcohols.[31] To be more specific, the sizes of ZnO quantum dots prepared using methanol, ethanol and hexanol under similar experimental conditions are 3.3, 5.6 and 7.8 nm, respectively. This finding can be explained by the above highlighted growth mechanism, thus making it reasonable.

To evaluate the potential applicability in gas sensors for n-butanol gas, we investigated fundamental gas sensing properties of the as-synthesized ZnO nanoparticles. The sensing performances of a sensor not only depend on the gas atmosphere but also on the operating temperature. To be more specific, there exists a range of temperatures for the sensor that result in the highest gas response when the other conditions remain the same.[19,25] Fig. S3† shows the variation of resistance with temperature, and a typical negative temperature coefficient of resistance can be found. Fig. S4† shows the temperature dependence of gas response for the investigated sensor. One can see that 320 °C is the optimal operating temperature for the

as-fabricated ZnO nanocrystalline powder gas sensor. Fig. 4(a) displays the dynamic response to different n-butanol concentrations from 10 to 1000 ppm in dry air at an operating temperature of 320 °C. Before n-butanol gas is injected, the gas response remains stable without any big fluctuations. Once the gas is injected, the gas response increases fast and almost reaches its constant. When the sensor is exposed to ambient air again, the response value decreases rapidly to the baseline. And one can also find that the sensor based on ZnO nanoparticles has a good response to the n-butanol gas. It can detect a concentration as low as 10 ppm toward which the gas response is 4.3. Its gas response to 100, 300, 500, 700 and 1000 ppm n-butanol gas is 62, 368, 805, 1237 and 1988, respectively. As we have discussed in the introduction, the maximum acceptable concentration of n-butanol in working shops is stipulated as 152–303 mg m^{-3}, which corresponds to 45–90 ppm, and the lower explosive limit is l.45% by volume, which corresponds to 14 500 ppm. Hence, the fabricated gas sensor based on ZnO nanoparticles is extremely sensitive toward n-butanol gas, and its gas response satisfies the detection needs of n-butanol in aspects of noxious and inflammable gas.

The gas response to n-butanol at an operating temperature of 320 °C also shows a good linear dependence on the gas concentration. As shown in Fig. 4(b), the line for n-butanol is the calibration curve and the experimental data were fitted as:

$$\beta = 2.077C - 171.282. \tag{1}$$

The low detection limit is calculated as 82.95 ppm according to this equation, but the sensor can easily detect as low as 10 ppm
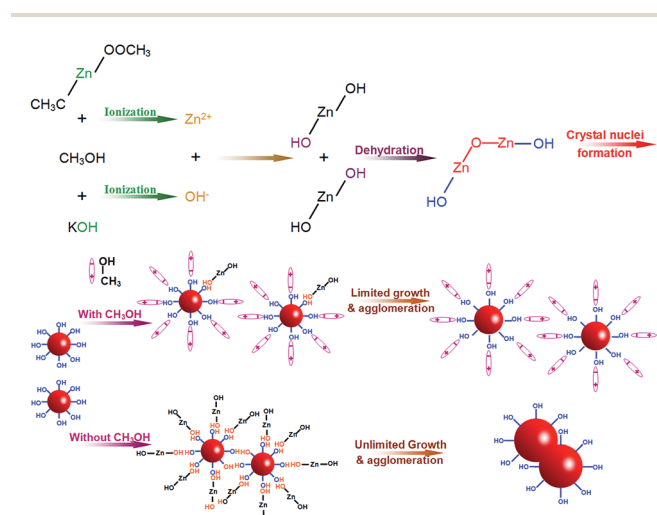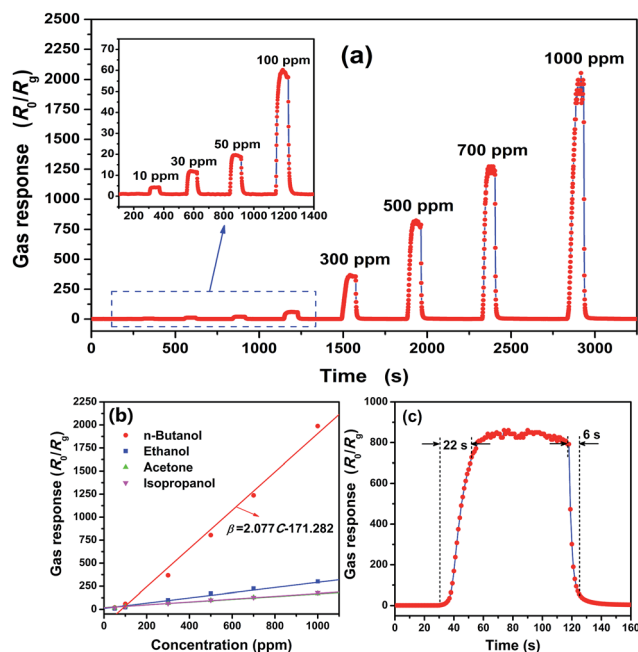

Fig. 4   The dynamic response to different n-butanol concentrations from 10 to 1000 ppm in dry air (a), the variation of sensor response to different concentrations of target gases (b), and the dynamic response to 500 ppm n-butanol gas in dry air (c) at an operating temperature of 320 °C.

Fig. 3   Schematic illustration of the formation process for the ZnO nanoparticles.

(Fig. 4(a)). This means that eqn (1) is not suitable for the low concentrations. Hence, another equation based on the experimental data (Fig. 4(a)) obtained at concentrations lower than 100 ppm was fitted as:

$$\beta = 0.382C + 0.458. \qquad (2)$$

According to this equation, the low detection can be estimated to be 1.42 ppm, which is much more convincing. Notice that, the dependence between the gas response and concentration is described by a piecewise function, which is made up of eqn (1) and (2). Eqn (2) is suitable for low concentrations while eqn (1) suits high concentrations. The reasons why two different equations exist in different concentration ranges needs further investigations.

At the same time, the response to other common VOCs such as ethanol, acetone and isopropanol in different concentrations from 50 to 1500 ppm were also measured at 320 °C. The dynamic response–recovery curves are shown in Fig. S5† and summarized in Fig. 4(b). According to the corresponding fitted curves displayed in the same figure, all of them exhibit a good linear relationship. Compared with the gas response to *n*-butanol at the same concentration, the others are much lower. More specifically, the gas response to *n*-butanol is roughly 5.6, 10.6 and 10.0 times higher than that to ethanol, acetone and isopropanol gases, respectively, at a concentration of 1000 ppm. This means that the ZnO nanoparticles-based gas sensor has a good selectivity to *n*-butanol among the examined VOC gases.

The response and recovery times are also very important parameters for gas sensors. In Fig. 4(c), a magnifying dynamic response to 500 ppm *n*-butanol gas in dry air at an operating temperature of 320 °C is exhibited. Based on the definition of response and recovery times, they are calculated to be 22 and 6 seconds, respectively. Both of them illustrate fast response and recovery properties toward *n*-butanol gas of the as-fabricated sensor. Moreover, the repeatability of the as-fabricated gas sensor was also investigated by testing 500 ppm *n*-butanol five times at the same conditions and is shown in Fig. 5. It shows that all of the gas responses can reach 800 with only small fluctuations. To be more specific, the error limit is only 4.2%, and the response as well as the recovery time do not show much difference. So, the sensor based on ZnO nanoparticles shows good repeatability. Not only that, the stability of the gas sensor was also verified by testing the gas response toward 500 ppm *n*-butanol over 25 days. The gas response evolution is shown in Fig. 6, and one can find that the response only has a small fluctuation, which is below 7.3% of its initial value. This illustrates the good stability of the gas sensor.

Table 1 compares the sensing performance of the as-prepared ZnO nanoparticles against previously reported metal oxide semiconductor-based sensors toward *n*-butanol gas. The extremely high response, which is 630 at 150 °C for 10 ppm *n*-butanol gas was reported for mesoporous SnO₂ prepared with hydrothermal treatment.[3] However the recovery time is poor, and it is hard for the sensor to recover to the initial state after exposure to the air until an additional heating treatment at 300 °C is used. Even with the heating treatment, it still needs more
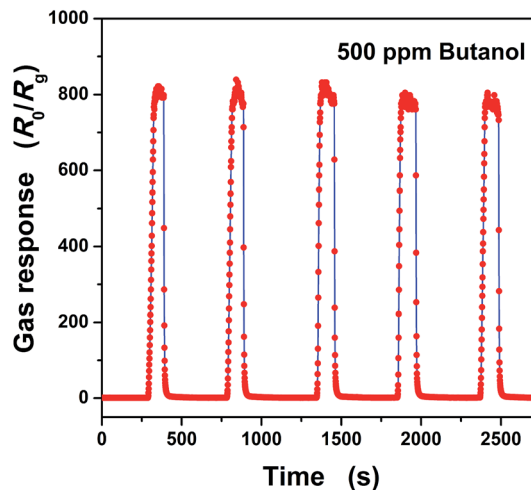

Fig. 5 Dynamic response–recovery cycles of the as-fabricated gas sensor toward 500 ppm *n*-butanol gas at an operating temperature of 320 °C.

than 120 s to return to the initial working state, which is not satisfied, with the need of real time monitoring. Apart from the mesoporous SnO₂ reported by Wang,[3] the as-fabricated sensor has the highest sensitivity. Moreover, most reported sensors reach their saturation in a concentration lower than 500 ppm,[15,16,18,19,23] and it is hard for the sensors to reflect concentrations which are higher than their saturation concentration. But the sensor in this work shows a pretty good linear relationship in a wide range from 10 ppm to 1000 ppm, or even higher.

The principle of *n*-butanol detection of the as-fabricated sensor is based on its conductance variation, which can be interpreted by Wolkentein's model,[32,33] as shown in Fig. 7. Oxygen species in the air are adsorbed on the ZnO particle surface and ionized to adsorbed oxygen ions (O_{ads}^- and O_{ads}^{2-})
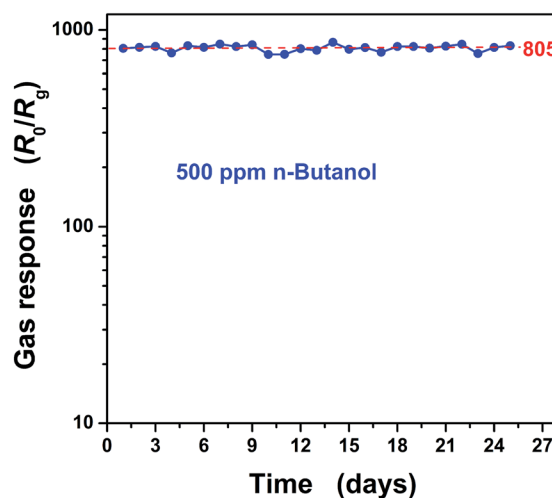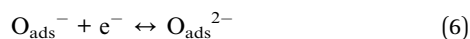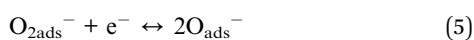

Fig. 6 Dynamic response–recovery cycles of the as-fabricated gas sensor toward 500 ppm *n*-butanol gas at an operating temperature of 320 °C.
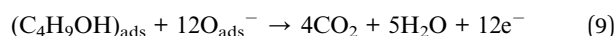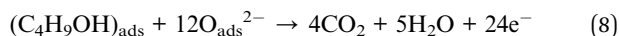
Table 1 Comparison of the sensing performances of various semiconductor metal oxide-based gas sensors toward *n*-butanol

Materials	Concentration (ppm)	Operating temperature (°C)	Sensitivity	Ref.
Mesoporous SnO_2	10	150	630	3
ZnO nanoflakes	500	330	87	14
Au/ZnO nanowires	400	320	28	15
ZnO microflowers	100	320	24.1	16
ZnO/α-Fe_2O_3 nanorods	100	225	57	18
SnO_2 nanospheres	100	120	32.3	19
α-Fe_2O_3 hollow spindles	100	280	13.9	20
$ZnSnO_3$ cubes	100	300	9	21
NiO hollow microspheres	500	350	2.5	23
ZnO nanoparticles	100	320	62	This work
	500		805	

by capturing free electrons from the particles, which leads to the formation of a thick space-charge layer and a consequent high resistance of the sensor. This process can be described using the following equations:

$$O_{2gas} \leftrightarrow O_{2ads} \tag{3}$$

$$O_{2ads} + e^- \leftrightarrow O_{2ads}^- \tag{4}$$

$$O_{2ads}^- + e^- \leftrightarrow 2O_{ads}^- \tag{5}$$

$$O_{ads}^- + e^- \leftrightarrow O_{ads}^{2-} \tag{6}$$

When the sensor was exposed to *n*-butanol gas, *n*-butanol would react with O_{ads}^- or O_{ads}^{2-} to form CO_2 and H_2O. And the electrons captured by O_{ads}^- or O_{ads}^{2-} would be released again, which results in the thinning of the space-charge layer and a decrease of the potential barrier. This process leads to a decrease of the resistance and can be expressed as follows:[18,23]

$$(C_4H_9OH)_{gas} \leftrightarrow (C_4H_9OH)_{ads} \tag{7}$$

$$(C_4H_9OH)_{ads} + 12O_{ads}^{2-} \rightarrow 4CO_2 + 5H_2O + 24e^- \tag{8}$$

$$(C_4H_9OH)_{ads} + 12O_{ads}^- \rightarrow 4CO_2 + 5H_2O + 12e^- \tag{9}$$

According to the analysis of the possible gas sensing mechanism, one can find that O_{ads}^- and O_{ads}^{2-} have a great influence on the gas sensing properties of the ZnO nanoparticles. The

existence of the formed adsorbed oxygen ions can be easily detected by X-ray photoelectron spectroscopy (XPS). Hence, XPS was carried out, and the results are shown in Fig. S6.† From Fig. S6(a),† the Zn2p spectra reveal two peaks of $Zn2p_{3/2}$ and $Zn2p_{1/2}$ at 1021.4 eV and 1044.4 eV, respectively, with a good symmetry, which indicate that Zn in the particles is in a single form of Zn^{2+}. The splitting of the 2p doublet is 23.0 eV, which is in good agreement with the energy splitting reported for ZnO and corresponds to the 2p binding energy of Zn(II) (indexed Standard ESCA Spectra of the Elements and Line Energy Information, Φ Co., USA).[34] Fig. S6(b)† shows the O1s XPS spectra, where one can find that there are two components of oxygen varying in chemical states with O_{latt} (530.16 eV) and O_x^- (531.70 eV). O_{latt} is attributed to oxygen ions in the crystal lattice, which is thought to be pretty stable and have no contribution to the gas response. On the other hand, O_x^- is the adsorbed oxygen ion, which is mainly discussed in the gas sensing mechanism section in the oxygen deficient regions such as the oxygen vacancy (V_O), oxygen interstitial (O_i), and oxygen antisite (O_{Zn}).[11] To some degree, the peak area ratio of O_x^- and O_{latt} can represent the related concentrations of these two kinds of oxygen chemical states. In this work, that ratio of the as-prepared ZnO nanoparticles is calculated to be 0.66, which means a high concentration of O_x^- in the as-prepared ZnO nanoparticles.

The high response, fast response–recovery of the as-fabricated sensor toward *n*-butanol gas is thought to be attributed to the high specific surface area (81.0 m² g⁻¹) and the high concentration of O_x^-. As we have introduced, the gas sensing properties of semiconductor metal oxides are based on the reactions between gases and O_x^- belonging to sensing materials. A higher specific surface area brings a greater contact area between the gases and the metal oxide, which not only benefits to a fast gas diffusion, leading to a quick response and recovery, but is also helpful to have more O_x^- exposed to react with the gases. According to the chemical reaction kinetics, a higher reactant (O_x^-) concentration will naturally cause a faster reaction rate and higher reaction extent. At the same time, the high specific surface area and high concentration of O_x^- should be responsible for the higher sensitivity of the as-prepared ZnO nanoparticles compared to those of the other nanostructures
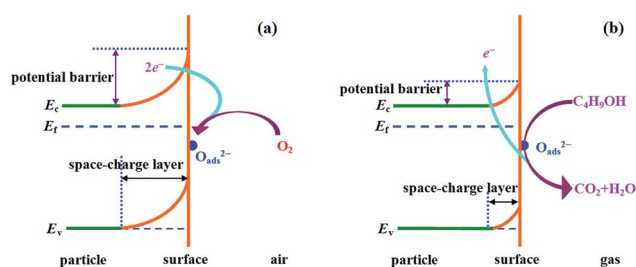

Fig. 7 A schematic diagram of the proposed reaction mechanism of the ZnO-based sensor to *n*-butanol in air (a) and in *n*-butanol (b).

listed in Table 1. However, the good selectivity and piecewise linear relationship between the response and concentration need further investigations.

4. Conclusions

ZnO nanoparticles were successfully synthesized by a simple low-temperature solvothermal method. The highly crystalline wurtzite-type ZnO nanoparticles with a particle size of 8.4 nm, a uniform near-sphere shape and high specific surface area were obtained. Such a small particle size and slight agglomeration are attributed to the use of methanol, which acts as both a solvent and an inhibitor of growth and agglomeration. The obtained ZnO nanoparticles were used directly to fabricate a gas sensor device which shows high-performance gas sensing properties including high sensitivity, good selectivity, fast response–recovery times, good repeatability and stability toward n-butanol gas. The high performance is attributed to its high specific surface area and high concentration of O_x^-, which resulted from the small grain size. Such a sensor based on ZnO nanoparticles is very promising a practical detector designed for n-butanol gas.

Acknowledgements

Notes and references

1 M. R. R. Khan, B. H. Kang, S. H. Yeom, D. H. Kwon and S. W. Kang, *Sens. Actuators, B*, 2013, **188**, 689.

2 H. Nguyen and S. A. El-Safty, *J. Phys. Chem. C*, 2011, **115**, 8466.

3 H. Wang, Y. Qu, H. Chen, Z. D. Lin and K. Dai, *Sens. Actuators, B*, 2014, **201**, 153.

4 A. B. Djurišić and Y. H. Leung, *Small*, 2006, **2**, 944.

5 H. Hagendorfer, K. Lienau, S. Nishiwaki, C. M. Fella, L. Kranz, A. R. Uhl, D. Jaeger, L. Luo, C. Gretener, S. Buecheler, Y. E. Romanyuk and A. N. Tiwari, *Adv. Mater.*, 2014, **26**, 632.

6 T. Meron and G. Markovich, *J. Phys. Chem. B*, 2005, **109**, 20232.

7 Y. Z. Jin, J. P. Wang, B. Q. Sun, J. C. Blakesley and N. C. Greenham, *Nano Lett.*, 2008, **8**, 1649.

8 N. Satio, H. Haneda, T. Sekiguchi, N. Ohashi, I. Sakaguchi and K. Koumoto, *Adv. Mater.*, 2002, **14**, 418.

9 M. H. Huang, S. Mao, H. Feick, H. Yan, Y. Wu, H. Kind, E. Weber, R. Russo and P. Yang, *Science*, 2001, **292**, 1897.

10 S. J. Pearton, D. P. Norton, K. Ip, Y. W. Heo and T. Steiner, *Prog. Mater. Sci.*, 2005, **50**, 293.

11 X. Y. Cai, D. Hu, S. J. Deng, B. Q. Han, Y. Wang, J. M. Wu and Y. D. Wang, *Sens. Actuators, B*, 2014, **198**, 402.

12 J. Zhang, S. Wang, M. J. Xu, Y. Wang, B. Zhu, S. Zhang, W. Huang and S. Wu, *Cryst. Growth Des.*, 2009, **9**, 3532.

13 C. Dong, X. Liu, X. Xiao, G. Chen, Y. Wang and I. Djerdj, *J. Mater. Chem. A*, 2014, **2**, 20089.

14 Y. V. Kaneti, J. Yue, X. Jiang and A. Yu, *J. Phys. Chem. C*, 2013, **117**, 13153.

15 C. Gu, L. Shanshan, J. Huang, C. Shi and J. Liu, *Sens. Actuators, B*, 2013, **177**, 453.

16 J. Huang, Y. Wu, C. Gu, M. Zhai, K. Yu, M. Yang and J. Liu, *Sens. Actuators, B*, 2010, **146**, 206.

17 L. Wang, S. Wang, H. Zhang, Y. Wang, J. Yang and W. Huang, *New J. Chem.*, 2014, **38**, 2530.

18 Y. V. Kaneti, Q. M. D. Zakaria, Z. Zhang, C. Chen, J. Yue, M. Liu, X. Jiang and A. Yu, *J. Mater. Chem. A*, 2014, **2**, 13283.

19 H. Zhang, Q. He, X. Zhu, D. Pan, X. Deng and Z. Jiao, *CrystEngComm*, 2012, **14**, 3169.

20 J. Huang, M. Yang, C. Gu, M. Zhai, Y. Sun and J. Liu, *Mater. Res. Bull.*, 2011, **46**, 1211.

21 J. Huang, X. Xu, C. Gu, W. Wang, B. Geng, Y. Sun and J. Liu, *Sens. Actuators, B*, 2012, **171–172**, 572.

22 J. Huang, X. Xu, C. Gu, M. Yang, M. Yang and J. Liu, *J. Mater. Chem.*, 2011, **21**, 13283.

23 G. Zhu, C. Xi, H. Xu, D. Zheng, Y. Liu, X. Xu and X. Shen, *RSC Adv.*, 2012, **2**, 4236.

24 J. Xu, Q. Pan, Y. Shun and Z. Tian, *Sens. Actuators, B*, 2000, **66**, 277.

25 Y. D. Wang, I. Djerdj, M. Antonietti and B. Smarsly, *Small*, 2008, **4**, 1656.

26 L. E. Greene, B. D. Yuhas, M. Law, D. Zitoun and P. Yang, *Inorg. Chem.*, 2006, **45**, 7535.

27 L. E. Greene, M. Law, J. Goldberger, F. Kim, J. C. Johnson, Y. Zhuang, R. J. Saykally and P. Yang, *Angew. Chem., Int. Ed.*, 2003, **42**, 3031.

28 L. R. Singh, R. S. Ningthoujam and S. D. Singh, *J. Alloys Compd.*, 2009, **487**, 466.

29 A. Kawska, P. Duchstein, O. Hochrein and D. Zahn, *Nano Lett.*, 2008, **8**, 2336.

30 S. Xu and Z. L. Wang, *Nano Res.*, 2011, **4**, 1013.

31 X. Liu, X. X. Xing, Y. X. Li, N. Chen, I. Djerdj and Y. D. Wang, *New J. Chem.*, 2015, **39**, 2881.

32 T. Wolkenstein, *Electronic Processes on Semiconductor Surface during Chemisorption*, Consultants Bureau, New York, 1991, p. 35.

33 T. Chen, Q. J. Liu, Z. L. Zhou and Y. D. Wang, *Nanotechnology*, 2008, **19**, 095506.

34 C. D. Wagner, W. M. Riggs, L. E. Davis, J. F. Moulder and G. E. Muilenberg, *Handbook of X-ray Photoelectron Spectroscopy*, PerkinElmer, Prairie, 1979, p. 80.